Nanoscale

Dynamic Article Links

Cite this: *Nanoscale*, 2011, **3**, 2627

www.rsc.org/nanoscale

PAPER

Cellular uptake mechanisms of functionalised multi-walled carbon nanotubes by 3D electron tomography imaging†

Khuloud T. Al-Jamal,[ab] Hannah Nerl,[c] Karin H. Müller,[d] Hanene Ali-Boucetta,[a] Shouping Li,[e] Peter D. Haynes,[c] Joerg R. Jinschek,[f] Maurizio Prato,[g] Alberto Bianco,[e] Kostas Kostarelos*[a] and Alexandra E. Porter*[c]

Received 20th January 2011, Accepted 23rd March 2011
DOI: 10.1039/c1nr10080g

Carbon nanotubes (CNTs) are being investigated for a variety of biomedical applications. Despite numerous studies, the pathways by which carbon nanotubes enter cells and their subsequent intracellular trafficking and distribution remain poorly determined. Here, we use 3-D electron tomography techniques that offer optimum enhancement of contrast between carbon nanotubes and the plasma membrane to investigate the mechanisms involved in the cellular uptake of shortened, functionalised multi-walled carbon nanotubes (MWNT–NH_3^+). Both human lung epithelial (A549) cells, that are almost incapable of phagocytosis and primary macrophages, capable of extremely efficient phagocytosis, were used. We observed that MWNT–NH_3^+ were internalised in both phagocytic and non-phagocytic cells by any one of three mechanisms: (a) individually *via* membrane wrapping; (b) individually by direct membrane translocation; and (c) in clusters within vesicular compartments. At early time points following intracellular translocation, we noticed accumulation of nanotube material within various intracellular compartments, while a long-term (14-day) study using primary human macrophages revealed that MWNT–NH_3^+ were able to escape vesicular (phagosome) entrapment by translocating directly into the cytoplasm.

Introduction

Chemically functionalised carbon nanotubes (*f*-CNTs) exhibit interesting properties that are attracting increasing attention as novel delivery systems for many diagnostic and therapeutic applications.[1,2] The hollow interior space and high aspect ratio of CNTs offer great advantages over existing delivery vectors, particularly since their high surface area can provide multiple attachment sites for drugs and targeting ligands.[3–5] Recently, our laboratories as well as others have reported that CNTs can act as delivery systems for drugs (methotrexate, amphotericin B),[6,7] antigens and genes (peptides, plasmid DNA, siRNA)[8–12] into prokaryotic and mammalian cells. We have also reported the uptake of various types of *f*-CNTs into a variety of cell types, and have shown that functionalised multi-walled carbon nanotubes (MWNTs) are non-cytotoxic,[13] while surface chemical functionalisation was shown to enhance cellular uptake, possibly affecting the degree and mechanism of its entry into cells.[9,14] The ability of CNTs to readily traverse the plasma membrane and enter the cell cytoplasm makes them very attractive candidate vectors, especially for the intracellular delivery of diagnostic and therapeutic agents, whereby escape from the endosomal compartment is considered a critical parameter for success.

Two dimensional transmission electron microscopy (2D TEM) has shown that ammonium functionalised MWNTs can directly translocate through the plasma membrane and internalise inside the cytoplasm.[15] We have also reported that non-functionalised single-walled carbon nanotubes (SWNTs) were able to cross the lysosomal membrane of mature human monocyte-derived macrophages (HMMs) and enter the cell cytoplasm.[16,17] The biophysical basis for the capability of CNTs to translocate through lipid bilayers has also been supported independently by others using coarse-grained molecular dynamics simulations.[18]

[a]*Nanomedicine Laboratory, Centre for Drug Delivery Research, The School of Pharmacy, University of London, London, WC1N 1AX, UK. E-mail: kostas.kostarelos@pharmacy.ac.uk; Fax: +44 (0)207-753-5942; Tel: +44 (0)207-753-5861*

[b]*Institute of Pharmaceutical Science, King's College London, Franklin-Wilkins Building, London, SE1 9NH, UK*

[c]*Department of Materials, Imperial College London, South Kensington, London, SW7 2AZ, UK. E-mail: a.porter@imperial.ac.uk; Fax: +44 (0)-207-5946757; Tel: +44 (0)207-5949691*

[d]*Multi-Imaging Centre, Department of Physiology, Development and Neuroscience, University of Cambridge, Cambridge, CB2 3DY, UK*

[e]*CNRS, Institut de Biologie Moléculaire et Cellulaire, UPR 9021 Immunologie et Chimie Thérapeutiques, 67000 Strasbourg, France*

[f]*FEI Company, Europe nanoPort, Achtseweg Noord, Eindhoven, The Netherlands*

[g]*Center of Excellence for Nanostructured Materials, Department of Pharmaceutical Sciences, University of Trieste, 34127 Trieste, Italy*

† Electronic supplementary information (ESI) available: See DOI: 10.1039/c1nr10080g

This journal is © The Royal Society of Chemistry 2011

On the other hand, other investigators have reported that lipopolymer (polyethylene glycol–phosphatidyl ethanolamine; PEG–PE) coated SWNTs[8] are uptaken by mammalian cells through endocytotic processes alone, disputing the ability of CNTs to translocate through the plasma membrane and internalise into the cytoplasm. More recently, Mu *et al.*[19] reported by also using 2D TEM that the uptake of carboxylated and amidated MWNTs by HEK293 non-phagocytic cells occurred *via* two processes: (a) direct translocation of individualised nanotubes through the plasma membrane; and (b) by uptake of *f*-MWNTs bundles *via* energy-dependent endocytotic mechanisms.

Previous experimental electron microscopy investigations of such phenomena mainly consisted of bright-field (BF) TEM of stained thin sections able to show individual *f*-MWNTs at the plasma membrane or clusters of *f*-MWNTs within lysosomes. However, BF-based imaging alone of intracellular *f*-CNTs is challenging due to the low inherent contrast, the demands on spatial resolution and the poor stability of ultrathin resin embedded sections under the electron beam. Further, conventional 2-D BF imaging is not able to offer confirmation whether the *f*-CNTs directly insert through the plasma membrane, or are membrane-bound, or simply lie on the surface of the TEM section. For such reasons, there exists a need for high-resolution 3D microscopy imaging techniques to attempt further elucidation of the interaction between *f*-MWNTs and cellular membranes by enhancing the contrast between the carbon nanotube backbone and the osmium-rich membranes. In this way it is also confirm whether nanotubes are capable of translocating through the plasma membrane.[15] Here we employ a combination of 3D electron tomography and high angle annular dark field scanning transmission electron microscopy (HAADF-STEM)—a technique highly sensitive to local atomic number variations—to enhance contrast from stained cell membranes. The position of the CNTs in relation to cell membranes can be confirmed using energy-filtered TEM (EFTEM)—a method that yields characteristic energy-loss information—by mapping the nanotubes at the carbon *K* edge and the osmium tetroxide stained cell membranes at the osmium $N_{4,5}$ edge. The combination of these techniques is considered critical towards assessment and confirmation as to whether the CNTs were able to directly translocate through cellular membranes.

Experimental

Materials

Pristine MWNT was purchased from Nanostructured & Amorphous Materials Inc. (Houston) at 94% purity (stock no. 1240XH). Their outer diameter was between 20 and 30 nm, and length was between 0.5 and 2 μm. Chemicals and solvents were obtained from Sigma-Aldrich (USA) and they were used as received. F12 Ham media, Macrophage Serum-Free Medium Mø-SFM, fetal bovine serum (FBS), penicillin/streptomycin, and phosphate buffered saline (PBS) were from Gibco, Invitrogen (UK). LymphoPrep was obtained from Axis-Shields (Oslo, Norway).

Chemical functionalisation of MWNT

Ammonium functionalised (MWNT–NH_3^+) were synthesised as follows: oxidized MWNTs were obtained following the procedure reported in reference (Li, Wu *et al.*, 2008),[20] (200 mg) were heated in 10 ml of neat oxalyl chloride at 62 °C for 24 h. After evaporation *in vacuo* the resulting nanotubes were dispersed in a solution of Boc-monoprotected diamino-triethyleneglycol (TEG) (530 mg) in distilled THF (15 ml) and heated at reflux for 48 h (Wu, Wieckowski *et al.*, 2005).[6] The nanotubes were re-precipitated several times from methanol/diethyl ether by successive sonication and centrifugation. The Boc protecting groups were removed overnight using 4 M HCl in dioxane (20 ml) to afford MWNT–NH_3^+ (185 mg) following evaporation of the acid solution and re-precipitation in diethyl ether. The Kaiser test afforded a loading of 320 μmol g^{-1} of amino groups.

Lung epithelial (A549) cell culture

Epithelial lung carcinoma cells (A549; ATCC®, CCL-185™) were maintained and passaged in F12 Ham media, supplemented with 10% FBS, 50 U ml^{-1} penicillin, 50 μg ml^{-1} streptomycin, 1% L-glutamine and 1% non-essential amino acids, at 37 °C in 5% CO_2. Cells were passaged twice a week using TrypLE Express at 80% confluency.

Isolation of human monocyte-derived macrophage (HMM) cell culture

HMM cells were obtained by *in vitro* culture of human monocytes isolated from human buffy coat residues (National Blood Service, Brentwood, UK). Buffy coat residue was washed once with PBS and the resulting cell sediment was mixed with an equal volume of fresh PBS. Thirty millilitres of diluted buffy coat residue was layered onto 15 ml of LymphoPrep and after centrifugation at 20 °C for 30 min at 700×*g*, the opaque interphase of mononuclear cells was removed and washed 3× with PBS containing 4 mg ml^{-1} Bovine Serum Albumin (BSA) to remove platelets. Then, monocytes were enriched by an additional centrifugation step in a Percoll gradient. Mononuclear cells were resuspended in 4 ml of PBS and mixed with 8 ml of Percoll: Hanks' Balanced Salt Solution (10× concentrate) (6 : 1, at pH 7.0). After centrifugation at 20 °C for 30 min at 450×*g*, the monocytes were collected from the top of the gradient, washed in PBS/BSA and seeded in 24 and 48-well tissue culture plates at about 1–2 × 10^6 cells per well and 0.5–1 × 10^6 cells per well respectively using Mø-SFM unless otherwise stated. For microscopy, cells were seeded on ethanol-sterilised glass coverslips (ø 13 mm) in 50 μl culture medium at a density of about 0.25–0.5 × 10^6 cells per coverslip. After incubation for 1 h at 37 °C, any remaining non-adherent cells were removed by washing twice with PBS. Adherent monocytes were cultured at 37 °C in 5% CO_2 using Mø-SFM supplemented with 100 U ml^{-1} penicillin and 100 μg ml^{-1} streptomycin for at least 6–7 days prior to experiments unless stated otherwise, renewing the culture medium twice a week.

Incubation of MWNT–NH_3^+ with cells

MWNT–NH_3^+ were used as sterile stock solutions at 0.5 mg ml^{-1} in 5% dextrose. Stock dispersion was bath sonicated for 15 min prior use in cell culture studies. Cells were incubated with 50 μg ml^{-1} of MWNT–NH_3^+ type at 37 °C for 24 hours and 4 h. Cells were kept on ice and refrigerated at 4 °C for 4 h to inhibit active uptake. Following incubations, free

 This journal is © The Royal Society of Chemistry 2011

MWNT–NH_3^+ were removed by washing 3× in ice-cold saline prior to fixation. The 4 h time point was selected to compare active and passive uptake effects, while a 24 h time point was chosen to simulate long term exposure. To establish the long-term fate of MWNT–NH_3^+ inside cells, HMMs were exposed to MWNT–NH_3^+ in a pulse-chase experiment. For all the pulse-chase experiments, cells were labelled with MWNT–NH_3^+ at 50 μg ml^{-1} for 4 h. Then, cells were washed and cultured in full cell culture medium in the absence of MWNT–NH_3^+ for a further 0 h, 24 h, 3 days, 7 days and 14 days prior to processing for TEM.

Transmission electron microscopy

Following the incubations, cells were rinsed briefly in saline (0.9% NaCl) to remove any non-ingested particles and were then fixed in 4% glutaraldehyde in 0.1% PIPES buffer, pH 7.2 for 1 h at 4 °C. After several rinses in deionised water (DIW), the selected samples were osmicated (1% OsO_4, 0.15% potassium ferricyanide; 2 mM $CaCl_2$ in DIW) for 1 h at RT. This osmication process also acts to enhance contrast from lipids inside the cell. Again, the samples were washed several times with DIW and then bulk stained for 1 h at RT in the dark using uranyl acetate. The osmication procedure was omitted for cells prepared for the temperature study and the pulse chase incubations. Following 2 washes in DIW, the sample was dehydrated in graded solutions of ethanol (70%, 95%, 100%), 3× in each for 5 minutes. After additional two washes in 100% acetonitrile, the sample was infiltrated with Quetol 651 resin over 4 days using fresh resin each day. Resin was cured at 60 °C for 24 h. Ultrathin sections (~70 nm) were cut onto distilled water with a Leica Ultracut ultramicrotome using a 35° wedge angle diamond knife. Sections were mounted on 300 mesh bare copper grids.

Sections were viewed in a FEI Titan 80–300 scanning/transmission electron microscope (S/TEM) operated at 300 kV. Bright field images in TEM mode, as well as high angle annular dark field images in STEM mode, were acquired. EFTEM was performed using a 10 μm objective aperture to optimise spatial resolution.[21] All HAADF-STEM experiments were performed using inner (θ_{in}) and outer (θ_{out}) HAADF collection angles of θ_{in} 32.5 mrad and θ_{out} 161.0 mrad to enhance atomic number contrast.

BF tomography sets were acquired over a tilt angle range of −50° and +50° at 2° increments. Each image was corrected for any shift relative to the reference image using a cross-correlation routine. Spatial and rotational alignment through the tilt series was corrected by sequential cross-correlation and series averaging. Three dimensional reconstruction was carried out using a simultaneous iterative reconstructions technique (SIRT)[21] using Inspect3D reconstruction software. The contrast in the BF reconstructions was inverted to compare with heavy metal stained sections imaged using HAADF STEM. Visualisation of the 3-D tomography reconstructions was performed using Amira 3D visualisation software (Mercury Computer Systems, France). No diffraction contrast from the CNTs was visible in the BF images, confirming that the BF images are suitable for tomographic reconstruction as the projection requirement was fulfilled.

Results and discussion

Prior to imaging the chemically modified MWNTs (MWNT–NH_3^+) within cells, their physicochemical characteristics were determined. MWNT–NH_3^+ were prepared following a two-step chemical treatment consisting of oxidation and subsequent introduction of amino groups by amidation of carboxyl groups. The nanotubes were initially treated under strong acid conditions to reduce their length below one micron.[20] The average length was evaluated by observing a series of TEM images and resulted between 50 and 500 nm. The carboxylic functional groups were subsequently transformed by acyl chloride activation and reaction with diaminotriethylene glycol to generate cationic MWNT–NH_3^+. The degree of amino group loading on the side walls and tips was determined by the Kaiser test and found to be 320 μmol g^{-1}. The diameter distribution obtained is shown in Fig. 1A. MWNT–NH_3^+ were bath sonicated in 5% dextrose before use to improve dispersion. High resolution lattice imaging confirmed the graphitic structure of the tubes had been preserved during functionalisation and length shortening, and that the catalyst had been removed, as previously shown[20] (Fig. 1B).

The interaction of MWNT–NH_3^+ with epithelial lung carcinoma cells (A549 cells) and mature human monocyte-derived macrophages (HMMs) as models of non-phagocytic and phagocytic cells respectively was carried out by exposing both cell types to 50 μg ml^{-1} of MWNT–NH_3^+ for 4 and 24 h. Cells were then fixed, embedded and thin sections were prepared for observation in the TEM. Bright field TEM (BF-TEM) images of unstained cell sections showed substantial uptake of MWNT–NH_3^+ by both cell types (Fig. 1C) after 4 h exposure. At 37 °C and 4 h incubation, MWNT–NH_3^+ were found associated with the cell membrane of A549 cells, and frequently as clusters or individualised CNTs within the endosomes and cytoplasm (Fig. 1C). After 24 h exposure to A549 cells, uptake appeared to be more extensive throughout the cells. In osmium tetroxide stained (osmicated) cell sections the MWNT–NH_3^+ were found inside endosomes, the cell cytoplasm and occasionally associated with organelles such as nucleus and mitochondria (Fig. S1†). In comparison, HMMs were able to phagocytose clusters of MWNT–NH_3^+ localised mostly within vesicles (presumably phagosomes). Individual nanotubes were also observed throughout the HMM cell (Fig. 1C). Overall, the cells appeared healthy at all time points.

In order to elucidate further whether the uptake process was energy-dependent, incubation with cells was carried out for 4 h at 4 °C and 37 °C, as energy deprivation could block any active uptake (energy-dependent) processes.[13] Energy depletion at 4 °C reduced, but not completely inhibited, CNT uptake particularly by HMMs where phagocytosis of large nanotube clusters appeared to have been inhibited (Fig. 1C, bottom panels). These results indicated that MWNT–NH_3^+ were able to internalise—even though to a lesser extent—inside both cells types at 4 °C in the absence of an active cellular uptake process. Notably, the amount of MWNT–NH_3^+ bound to the cell membrane of A549 cells at 4 °C was reduced while a dramatic reduction in uptake was observed for HMMs at 4 °C.

We then applied more advanced electron microscopy techniques focusing on the interaction between MWNT–NH_3^+ and the epithelial lung cell (A549) plasma and endosomal membranes

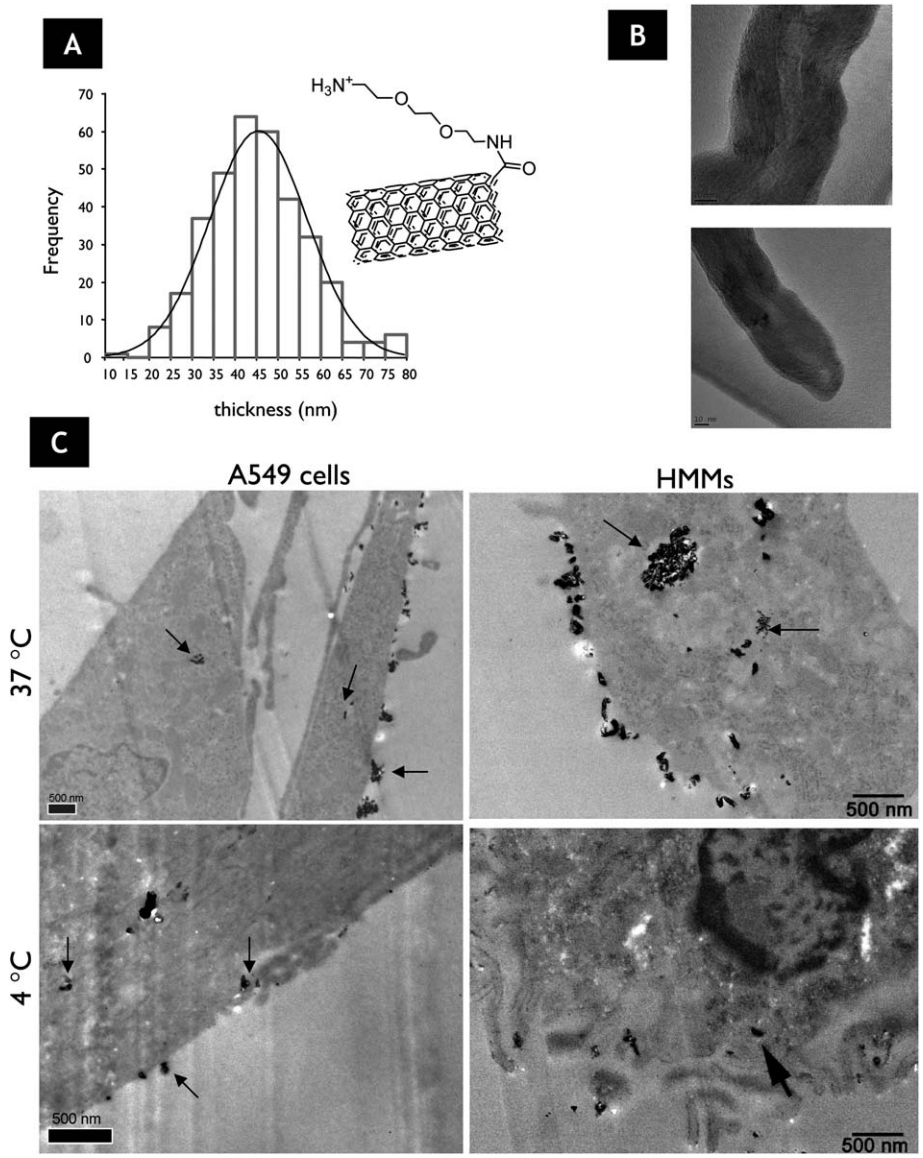

Fig. 1 Characterisation of MWNT–NH_3^+ and interaction with A549 cells and HMMs. (A) The chemical structure of MWNT–NH_3^+ and their diameter distribution; (B) high resolution bright-field (BF TEM) image showing that the lattice of individual carbon layers was preserved during functionalisation and shortening; and (C) BF TEM of unstained cell sections exposed to MWNT–NH_3^+ for 4 h at 37 °C or 4 °C, at 50 μg ml^{-1} concentration. At 37 °C, MWNT–NH_3^+ were found aligned perpendicular to the plasma membrane, as individual nanotubes or as small bundles within the A549 cells (top left), or within phagosomes of HMMs (top right). There was an overall reduction of uptake at 4 °C compared to 37 °C in both cell types (bottom images), however, TEM confirms cytoplasmic localisation of MWNT–NH_3^+ in A549 cells after incubation at 4 °C. MWNTs are indicated by black arrows.

after exposure to 50 μg ml^{-1} MWNT–NH_3^+ for 24 h. In osmicated cells, the MWNT–NH_3^+ were seen in an orientation 'end-on' to the plasma membrane of A549 cells, and occasionally inserting through the plasma membrane (Fig. 2 and 3, arrows). On further inspection, two types of interaction with the plasma membranes were identified: (a) MWNT–NH_3^+ were observed directly crossing through the plasma membrane (Fig. 2); and (b) MWNT–NH_3^+ wrapped by the plasma membrane were observed internalising into the cell (Fig. 3).

To confirm that the *f*-MWNTs were able to directly pierce the plasma membrane of A549 cells, 3D electron tomography was employed (Fig. 2C). Orthoslices through tomographic reconstruction illustrated that the MWNT–NH_3^+ inserted through the plasma membrane and extended into the cell cytoplasm (Fig. 2C and Movie S1†). Chemical analysis by EFTEM mapping was further used to distinguish the position of the carbon nanotube with respect to the lipid bilayer of the plasma membrane. EFTEM maps taken at the osmium $N_{4,5}$ edge (46 eV) confirmed that the MWNT–NH_3^+ were able to translocate through the plasma membrane without being surrounded by an osmium rich membrane (Fig. 2D). The bright, mottled layer that surrounded the *f*-MWNTs at the insertion site (Fig. 2A) implied that the heavy metal stain had bound to the surfaces of the *f*-MWNTs. The MWNT–NH_3^+ frequently appeared bright at the osmium edge indicating that they had been stained by the osmium (Fig. 2D, osmium map).

 This journal is © The Royal Society of Chemistry 2011

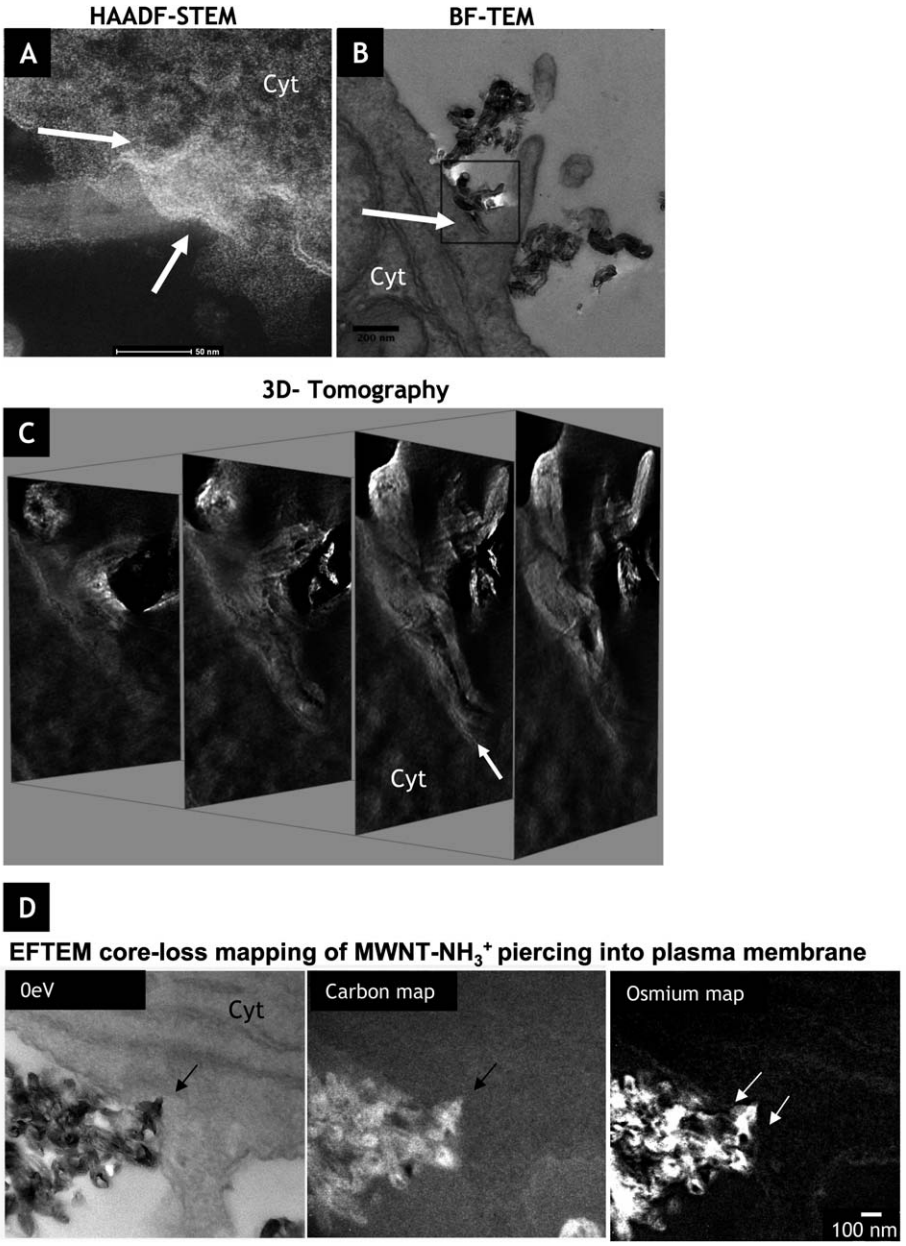

Fig. 2 MWNT–NH_3^+ breaking through the plasma membrane of stained A549 epithelial cells. (A) HAADF-STEM image showing MWNT–NH_3^+ inserting into the cell membrane of A549 cells; (B) BF-TEM image; (C) orthoslices taken at different heights through a tomographic reconstruction taken from the boxed region in (B). The tomogram shows the MWNT–NH_3^+ pierce the plasma membrane of a cell stained with osmium tetroxide. The left side of the MWNTs is covered by a bright membrane (arrow) whereas the right side of the MWNT interfaces directly with the cytoplasm; (D) EFTEM jump ratio maps taken using a 10 eV slit centred at 0 eV, the carbon *K* edge at 284 eV (pre-slit position 277 eV and post-slit 289 eV), and the osmium O edge (45 eV) (pre-slit 38 eV and post-slit 56 eV), showing the nanotube (black arrows) inserting into the cell membrane with no sign of membrane invagination. Incubation was performed at a concentration of 50 μg ml^{-1} of MWNTs at 37 °C for 24 h. The abbreviation "Cyt" was used to label the cytoplasm region to clarify the cell orientation.

The second type of interaction between the *f*-MWNTs and the plasma membranes observed, consisted of lipid membrane wrapping around an individual nanotube prior to cell internalisation. This process was illustrated clearly by HAADF-STEM and BF-TEM imaging (Fig. 3A and B) as well as by 3D tomography (Fig. 3C and Movie S2†). This observation is reminiscent of previous molecular modelling performed by Wallace and Sansom[23] who theoretically studied the interaction between CNT and a lipid bilayer membrane (DPPC bilayer) to model the CNT nanoinjection process performed by coarse-grained molecular dynamics. In their work, lipids from the bilayer coated both the inner and outer tube surfaces of CNTs which pierced into the membrane, with no apparent effect on bilayer integrity as the bilayer was able to self-seal. Based on the data obtained in the present study, membrane wrapping of the *f*-MWNTs does not seem to impede their cellular internalisation, however this may be different in the case of lipopolymer-, polymer- or other macromolecule-coated nanotubes. Further experimental and

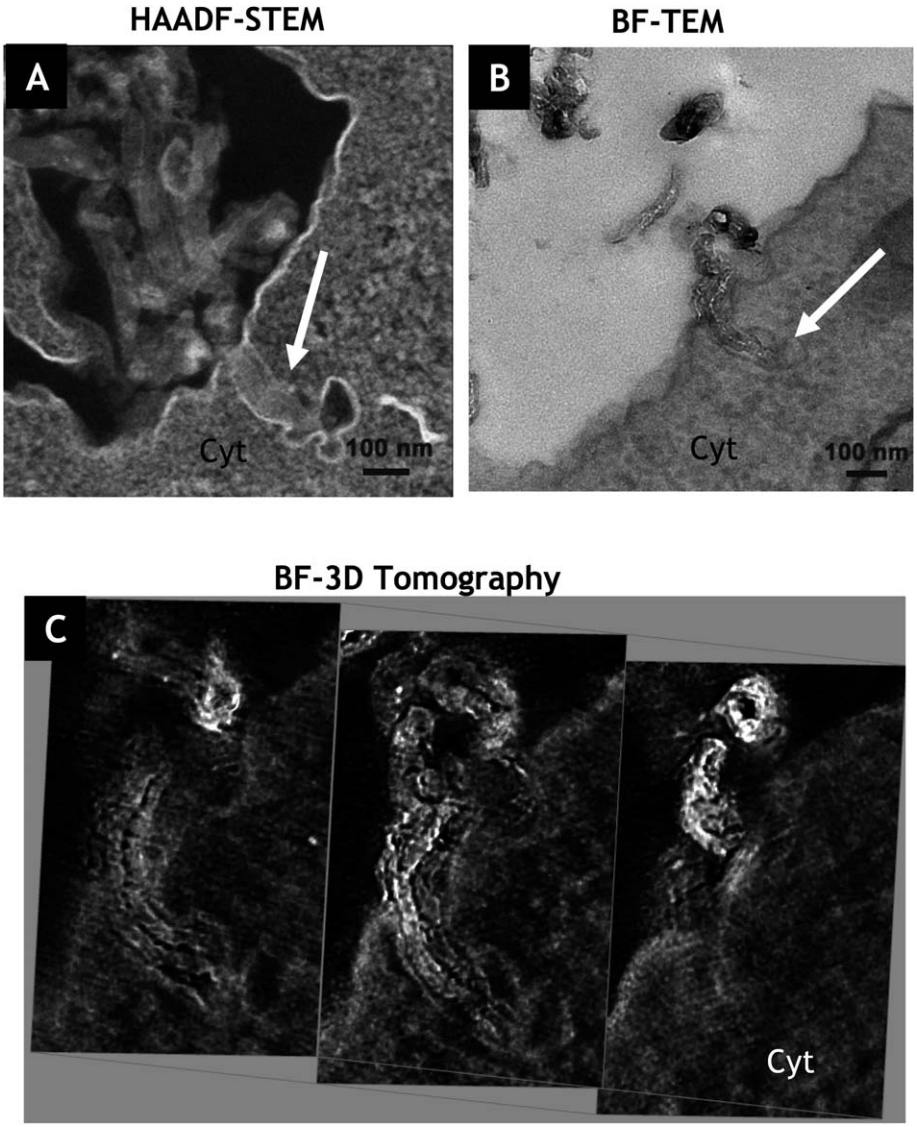

Fig. 3 MWNT–NH_3^+ crossing into A549 cells and wrapped by the plasma membrane of stained cells. (A) HAADF-STEM image showing a MWNT–NH_3^+ wrapped by the plasma membrane of A549 cells. (B) BF-TEM images of a similar region at the plasma membrane, and (C) orthoslices taken at different heights through a tomographic reconstruction taken from image (B) confirming that the plasma membrane surrounds the nanotube. Incubation was performed at 50 μg ml^{-1} concentration and 37 °C for 24 h. The abbreviation "Cyt" was used to label the cytoplasm region to clarify the cell orientation.

theoretical work will be needed in order to elucidate the parameters on which this lipid bilayer wrapping of individual nanotubes depends on (nanotube surface charge, grafting density, amphiphilic nature of surface functional groups).

We then attempted to study the intracellular trafficking characteristics of *f*-MWNTs to observe that the capacity of MWNT–NH_3^+ to pierce through lipid membranes was not exclusive to the outer plasma membrane. EFTEM maps of osmicated A549 cells indicated that MWNT–NH_3^+ localised within intracellular vesicular structures after 24 h exposure (Fig. 4A). This demonstrated that: (a) energetically active endocytic processes may also be responsible for internalisation, particularly of nanotube clusters as previously described;[19] or (b) individualised nanotubes that translocated directly into the cytoplasm may be captured, fused or accumulated within lipid-rich vesicular compartments (*e.g.* autophagosomes, mature endosomes, lysosomes). Three-window EFTEM maps taken at the osmium $N_{4,5}$ and carbon *K* edges showed individualised MWNT–NH_3^+ were able to traverse the endosomal membrane by "piercing" through and that they extended into the cell cytoplasm (Fig. 4A)—a process that has been recently described by others as "endosomal escape".[19] BF and EFTEM maps taken at the carbon *K* and osmium $N_{4,5}$ edges illustrated that many MWNT–NH_3^+ were also present within the cell cytoplasm of A549 cells and not surrounded by a membrane (Fig. 4B). We therefore propose that individualised *f*-MWNTs may be capable of translocating directly into the cytoplasm even after being internalised or associated with intracellular vesicular compartments by piercing their membrane.

To further confirm such observations, we repeated those investigations using short and long term exposures of

 This journal is © The Royal Society of Chemistry 2011

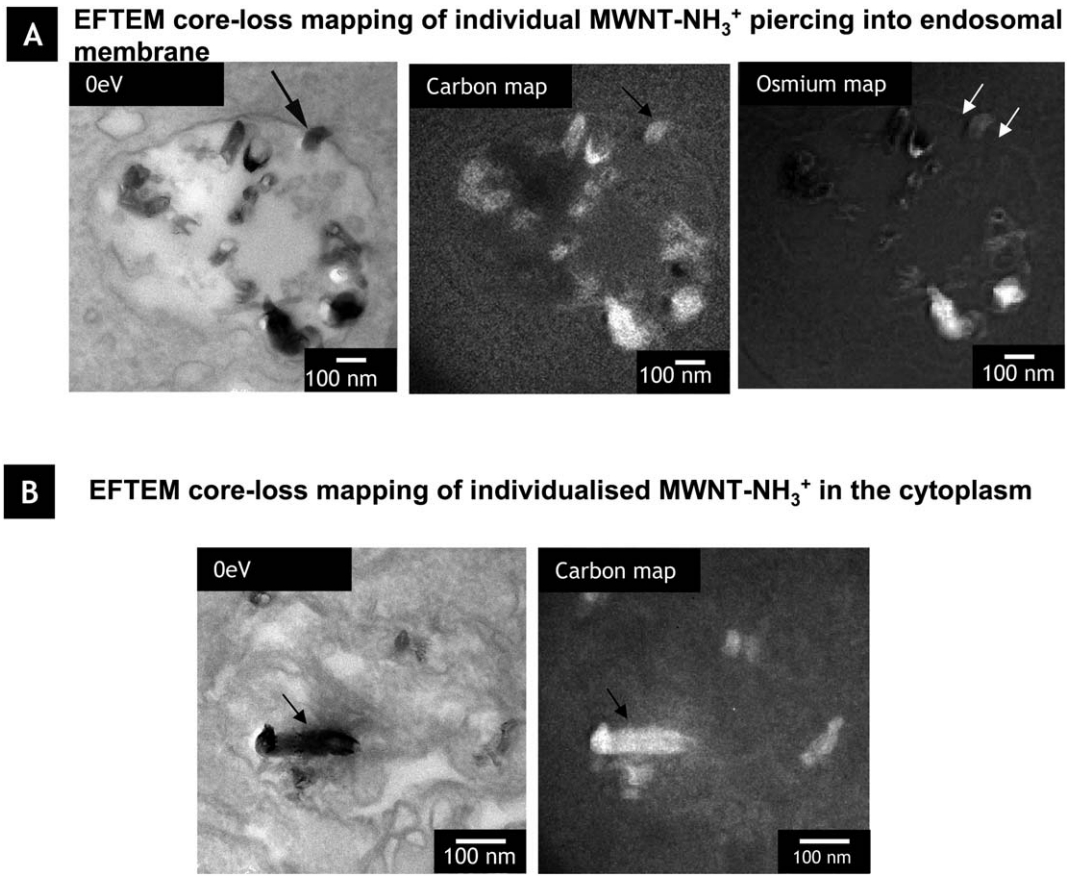

Fig. 4 Endosomal escape and cytoplasmic localisation of MWNT–NH_3^+ in stained A549 cells. (A) EFTEM maps taken with a 10 eV slit, at 0 eV, the carbon *K* edge and the osmium $N_{4,5}$ edge. Showing a nanotube (indicated by a black arrow) traversing through the endosomal membrane into the cell cytopalsm. (B) EFTEM maps of MWNT–NH_3^+ (black arrows) localised inside the cell cytoplasm of A549 cells. The CNTs are devoid of a membrane surrounding their surface. Incubation was performed at 50 μg ml^{-1} MWNT–NH_3^+ at 37 °C for 24 h.

phagocytosis proficient, non-dividing HMM cells to MWNTs. Interestingly, the capacity of MWNT–NH_3^+ for "endosomal-escape" was also seen in these cells, the predominant mechanism of nanotube internalisation within this cell type being the energetically active phagocytosis. HMMs were exposed to CNTs over 14 days in a pulse-chase experiment with 4 h incubation followed by fixation at 0 h, 24 h, 3 days, 7 days and 14 days. Up to 7 days (Fig. 5), the majority of MWNT–NH_3^+ were present as clusters inside phagosomes. However, after 14 days, nanotubes were localised individually throughout the cytoplasm (Fig. 5) confirming their capability to escape from the phagosomes.

Previously, we have shown that it is possible to visualise individual unlabelled fullerenes (C_{60}), SWNTs and MWNTs inside macrophage cells using a combination of EFTEM and 3D electron tomography techniques.[14,16,17,24] We have also demonstrated that low-loss EFTEM enables clear differentiation between SWNTs, C_{60} and cellular compartments in unstained sections.[17,21] 3D electron tomography has unambiguously shown the translocation of CNTs into intracellular compartments.[25] However, in these previous reports the carbon nanostructures studied were not chemically functionalised, therefore less compatible with the biological milieu and not as explored in biomedical applications. Here, using a combination of 3D TEM tomography and analytical microscopy techniques we have experimentally studied the interaction between chemically functionalised MWNTs and the plasma membrane of mammalian cells. It was demonstrated that ammonium functionalised MWNTs previously shown to enhance the delivery and biological activity of therapeutic agents,[4,10] could internalise within non-phagocytotic (A549) and phagocytotic (HMM) cells by direct translocation of the plasma membrane or by membrane wrapping of the individual nanotube. Internalisation by such processes required individual nanotubes and was energy-independent. On the other hand, nanotube bundles or clusters were found to be predominantly internalised by endocytotic processes that required energy. We therefore confirmed with powerful electron microscopy techniques that *f*-MWNTs are able to directly translocate through cellular membranes. Further investigations are warranted to compare the mechanism of cellular uptake and intracellular trafficking of negatively charged *f*-MWNT and the affinity of different types of *f*-MWNT for specific intracellular compartments (nucleus, mitochondria). Overall, the interplay between the cell types (*e.g.* phagocytotic or non-phagocytotic), the quality of the CNT dispersions (*e.g.* individualised or in clusters) and the nature of their surface modifications (*e.g.* macromolecule or small molecular weight functional groups) used in such studies play an extremely important role in determining the predominant mechanisms responsible for cellular uptake.

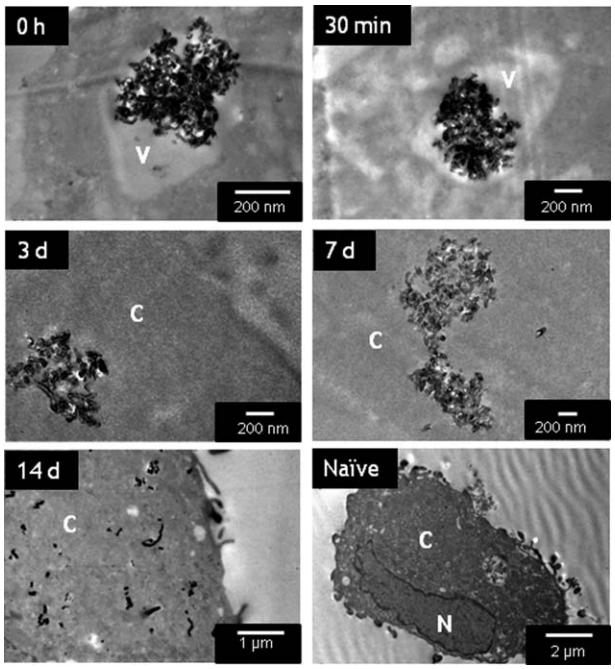

Fig. 5 Phagosome escape and cytoplasmic localisation of MWNT–NH_3^+ in unstained HMMs. Cells were incubated with MWNT–NH_3^+ for 4 h at 37 °C, at 50 µg ml^{-1} concentration. Then, cells were washed and either processed for BF-TEM immediately, or cultured on in cell culture medium for 30 min, 3, 7 days or 14 days. N, C, and V stands for nucleus, cytoplasm and vacuoles, respectively. After 7 d individual MWNT–NH_3^+ accumulated in the cytoplasm. After 14 d, individual CNTs dispersed in the cytoplasm.

The long term fate of CNTs following cellular uptake and cytoplasmic localisation also remains an important question of great interest both from the biomedical and the toxicological point of view. Strano and colleagues applied optical microscopy and single-particle tracking (SPT) to explore the fate of ssDNA-coated SWNTs following cellular uptake (into NIH-3T3 fibroblasts), and first reported evidence indicating CNT exocytosis after cellular internalisation.[26] There has also been recent evidence by various laboratories that some cell types may be able to degrade carbon nanotube structures.[27–29] Here we demonstrated that MWNT–NH_3^+ after 14 days of incubation with human macrophage cells were able to escape by membrane piercing from the intracellular vesicular compartments and appear predominantly as individualised nanotubes in the cytoplasm of healthy cells. Such "endosomal escape" was previously reported by Mu *et al.*[19] using a different cell line (kidney epithelial cells). Further work is required to determine the fate (exocytosis, degradation or accumulation) for given types of carbon nanotubes and cell types following nanotube intracellular translocation. Moreover, the challenge of translating such findings *in vivo* will critically define the limits in utilisation and safety of these interesting nanomaterials.

Acknowledgements

This work was supported partly by the European Union FP7 ANTICARB (HEALTH-2008-20157) research project, the Life Sciences Division FEI Company Eindhoven (AP), The Netherlands, the Centre for Electron Nanoscopy, the Danish Technical University, Lynby, DK, the National Research Fund Luxembourg (FNR), the Engineering and Physical Sciences Research Council for a Doctoral Training Account (HN) and the Titan Grant EPSRC (EP/C51596X). AB acknowledges the support of the CNRS and the Agence Nationale de la Recherche (grant ANR-05-JCJC-0031-01) and MP the University of Trieste MUR (cofin Prot. 2006035330) and Regione Friuli Venezia-Giulia. H. A.-B. wishes to acknowledge the Ministére de l'Enseignement Supèrieur et de la Recherche Scientifique (Algeria) for a scholarship.

References

1 A. Bianco, *Expert Opin. Drug Delivery*, 2004, **1**, 57.
2 K. Kostarelos, A. Bianco and M. Prato, *Nat. Nanotechnol.*, 2009, **4**, 627.
3 S. Y. Hong, G. Tobias, K. T. Al-Jamal, B. Ballesteros, H. A. Ali-Boucetta, S. Lozano-Perez, P. D. Nellist, R. B. Sim, C. Finucane, S. J. Mather, M. L. Green, K. Kostarelos and B. G. Davis, *Nat. Mater.*, 2010, **9**, 485.
4 M. Prato, K. Kostarelos and A. Bianco, *Acc. Chem. Res.*, 2008, **41**, 60.
5 J. Van den Bossche, W. T. Al-Jamal, B. Tian, A. Nunes, C. Fabbro, A. Bianco, M. Prato and K. Kostarelos, *Chem. Commun.*, 2010, **46**, 7379.
6 W. Wu, S. Wieckowski, G. Pastorin, M. Benincasa, C. Klumpp, J. P. Briand, R. Gennaro, M. Prato and A. Bianco, *Angew. Chem., Int. Ed.*, 2005, **44**, 6358.
7 C. Samori, H. Ali-Boucetta, R. Sainz, C. Guo, F. M. Toma, C. Fabbro, R. T. Da, M. Prato, K. Kostarelos and A. Bianco, *Chem. Commun.*, 2010, **46**, 1494.
8 N. W. Kam, Z. Liu and H. Dai, *Angew. Chem., Int. Ed.*, 2006, **45**, 577.
9 M. A. Herrero, F. M. Toma, K. T. Al-Jamal, K. Kostarelos, A. Bianco, R. T. Da, F. Bano, L. Casalis, G. Scoles and M. Prato, *J. Am. Chem. Soc.*, 2009, **131**, 9843.
10 J. E. Podesta, K. T. Al-Jamal, M. A. Herrero, B. Tian, H. Ali-Boucetta, V. Hegde, A. Bianco, M. Prato and K. Kostarelos, *Small*, 2009, **5**, 1176.
11 R. Singh, D. Pantarotto, D. McCarthy, O. Chaloin, J. Hoebeke, C. D. Partidos, J. P. Briand, M. Prato, A. Bianco and K. Kostarelos, *J. Am. Chem. Soc.*, 2005, **127**, 4388.
12 D. Pantarotto, C. D. Partidos, J. Hoebeke, F. Brown, E. Kramer, J. P. Briand, S. Muller, M. Prato and A. Bianco, *Chem. Biol.*, 2003, **10**, 961.
13 K. Kostarelos, L. Lacerda, G. Pastorin, W. Wu, S. Wieckowski, J. Luangsivilay, S. Godefroy, D. Pantarotto, J. P. Briand, S. Muller, M. Prato and A. Bianco, *Nat. Nanotechnol.*, 2007, **2**, 108.
14 A. E. Porter, M. Gass, J. S. Bendall, K. Muller, A. Goode, J. N. Skepper, P. A. Midgley and M. Welland, *ACS Nano*, 2009, **3**, 1485.
15 D. Pantarotto, R. Singh, D. McCarthy, M. Erhardt, J. P. Briand, M. Prato, K. Kostarelos and A. Bianco, *Angew. Chem., Int. Ed.*, 2004, **43**, 5242.
16 A. E. Porter, M. Gass, K. Muller, J. N. Skepper, P. A. Midgley and M. Welland, *Nat. Nanotechnol.*, 2007, **2**, 713.
17 J. Cheng, K. A. Fernando, L. M. Veca, Y. P. Sun, A. I. Lamond, Y. W. Lam and S. H. Cheng, *ACS Nano*, 2008, **2**, 2085.
18 C. F. Lopez, S. O. Nielsen, P. B. Moore and M. L. Klein, *Proc. Natl. Acad. Sci. U. S. A.*, 2004, **101**, 4431.
19 Q. Mu, D. L. Broughton and B. Yan, *Nano Lett.*, 2009, **9**, 4370.
20 S. Li, W. Wu, S. Campidelli, M. Prato, V. Sarnatskaïa, A. Tridon, A. Nikolaev, V. Nikolaev, A. Bianco and E. Snezhkova, *Carbon*, 2008, **46**, 1091.
21 O. L. Krivanek, M. K. Kundmann and K. Kimotok, *J. Microsc.*, 1995, **180**, 277.
22 P. Gilbert, *J. Theor. Biol.*, 1972, **36**, 105.
23 E. J. Wallace and M. S. Sansom, *Nano Lett.*, 2008, **8**, 2751.
24 A. E. Porter, M. Gass, K. Muller, J. N. Skepper, P. Midgley and M. Welland, *Environ. Sci. Technol.*, 2007, **41**, 3012.
25 C. Cheng, K. H. Muller, K. K. Koziol, J. N. Skepper, P. A. Midgley, M. E. Welland and A. E. Porter, *Biomaterials*, 2009, **30**, 4152.

 This journal is © The Royal Society of Chemistry 2011

26 H. Jin, D. A. Heller and M. S. Strano, *Nano Lett.*, 2008, **8**, 1577.
27 B. L. Allen, P. D. Kichambare, P. Gou, I. I. Vlasova, A. A. Kapralov, N. Konduru, V. E. Kagan and A. Star, *Nano Lett.*, 2008, **8**, 3899.
28 B. L. Allen, G. P. Kotchey, Y. Chen, N. V. Yanamala, J. Klein-Seetharaman, V. E. Kagan and A. Star, *J. Am. Chem. Soc.*, 2009, **131**, 17194.
29 V. E. Kagan, N. V. Konduru, W. Feng, B. L. Allen, J. Conroy, Y. Volkov, I. I. Vlasova, N. A. Belikova, N. Yanamala, A. Kapralov, Y. Y. Tyurina, J. Shi, E. R. Kisin, A. R. Murray, J. Franks, D. Stolz, P. Gou, J. Klein-Seetharaman, B. Fadeel, A. Star and A. A. Shvedova, *Nat. Nanotechnol.*, 2010, **5**, 354.